







Solar Cycle Observations of the Neon Abundance in the Sun-as-a-star

David H. Brooks^{1,6} , Deborah Baker² , Lidia van Driel-Gesztelyi^{2,3,4} , and Harry P. Warren⁵ 

¹ College of Science, George Mason University, 4400 University Drive, Fairfax, VA 22030, USA

² Mullard Space Science Laboratory, University College London, Holmbury St. Mary, Dorking, Surrey RH5 6NT, UK

³ Observatoire de Paris, LESIA, UMR 8109 (CNRS), F-92195 Meudon Principal Cedex, France

⁴ Konkoly Observatory of the Hungarian Academy of Sciences, Budapest, Hungary

⁵ Space Science Division, Naval Research Laboratory, Washington, DC 20375, USA

Received 2018 May 14; revised 2018 May 17; accepted 2018 May 17; published 2018 June 29

Abstract

Properties of the Sun’s interior can be determined accurately from helioseismological measurements of solar oscillations. These measurements, however, are in conflict with photospheric elemental abundances derived using 3D hydrodynamic models of the solar atmosphere. This divergence of theory and helioseismology is known as the “solar modeling problem.” One possible solution is that the photospheric neon abundance, which is deduced indirectly by combining the coronal Ne/O ratio with the photospheric O abundance, is larger than generally accepted. There is some support for this idea from observations of cool stars. The Ne/O abundance ratio has also been found to vary with the solar cycle in the slowest solar wind streams and coronal streamers, and the variation from solar maximum to minimum in streamers ($\sim 0.1\text{--}0.25$) is large enough to potentially bring some of the solar models into agreement with the seismic data. Here we use daily sampled observations from the EUV Variability Experiment on the *Solar Dynamics Observatory* taken in 2010–2014, to investigate whether the coronal Ne/O abundance ratio shows a variation with the solar cycle when the Sun is viewed as a star. We find only a weak dependence on, and moderate anti-correlation with, the solar cycle with the ratio measured around 0.2–0.3 MK falling from 0.17 at solar minimum to 0.11 at solar maximum. The effect is amplified at higher temperatures (0.3–0.6 MK) with a stronger anti-correlation and the ratio falling from 0.16 at solar minimum to 0.08 at solar maximum. The values we find at solar minimum are too low to solve the solar modeling problem.

Key words: stars: abundances – stars: corone – Sun: abundances – Sun: corona – Sun: transition region – Sun: UV radiation

1. introduction

The chemical composition of the Sun is a fundamental benchmark for many branches of astrophysics from solar system evolution to the heating of stellar corone. An accurate knowledge of solar elemental abundances is a prerequisite for many investigations, but our understanding of the solar composition has been called into question by our inability to reconcile helioseismological observations of the Sun’s interior with the predictions of theoretical models. This issue has become known as the “solar abundance problem,” and refers to the discrepancy introduced by upgraded calculations, which lowered the photospheric abundances of elements such as carbon, nitrogen, oxygen, and neon (Asplund et al. 2004). These elements are significant contributors to the opacity of the solar interior, so the reduced abundances also reduced the opacity of the radiative interior, and thus created a mismatch, for example, between the position of the base of the convective zone compared to that derived from helioseismic measurements (Bahcall et al. 2005a). Previously, the observations and models were in excellent agreement not only in the depth of the convection zone but also, for example, the sound speed profiles (Bahcall et al. 1997).

There can be little doubt that the revised abundances based on 3D numerical hydrodynamic models that relax assumptions such as local thermodynamic equilibrium in the spectral line formation, and utilize improved atomic data, are more realistic. They are able to capture the topology, spatial, and temporal

scales of solar granulation, for example (Nordlund et al. 2009), none of which could be reasonably modeled with the previous 1D hydrostatic simulations. While future improvements can be expected, such as incorporating the influence of photospheric magnetic fields that have only recently started to be included (Fabbian et al. 2010, 2012), attempts to solve the problem have focused on the abundances that are not inferred directly from the models.

While the photospheric abundances of carbon, nitrogen, and oxygen can be determined by comparison with the absorption lines they produce in the visible spectrum, there are no detectable neon lines. So the neon abundance is inferred indirectly by, for example, measuring the Ne/O abundance ratio using UV or X-ray spectra, and converting the ratio to a neon abundance using the known oxygen abundance. This makes the determination of the photospheric abundance of neon in the Sun much less certain than that of the other elements.

The measurements are further complicated by the first ionization potential (FIP) effect (Pottasch 1963). The composition of the solar photosphere and corona are different: elements with a low FIP (≤ 10 eV) are enhanced in the corona and slow speed solar wind by factors of 2–4, while high-FIP elements retain their photospheric abundances (Meyer 1985; Feldman et al. 1992). Since neon (FIP = 21.6 eV) and oxygen (FIP = 13.6 eV) are both usually assumed to be high-FIP elements, they are in principle unaffected. In some circumstances, however, variations are seen in different features such as quiescent active regions (Schmelz et al. 1996), and oxygen also apparently sometimes behaves like a low-FIP element with

⁶ Current address: *Hinode* Team, ISAS/JAXA, 3-1-1 Yoshinodai, Chuo-ku, Sagami-hara, Kanagawa 252-5210, Japan.

respect to neon in long-lived structures such as coronal streamers (Landi & Testa 2015), or the slow solar wind (Shearer et al. 2014).

Taking these issues into account, Antia & Basu (2005) and Bahcall et al. (2005b) proposed that if the photospheric abundance of neon were raised by a factor of 2.5 or more then the solar models would come back into agreement with the seismic observations. There is, however, no obvious reason to raise the neon abundance. The standard value for neon prior to the revision came from weighted means of solar wind, solar energetic particle, and flare spectra (Grevesse et al. 1996). Furthermore, the post-revision of Asplund et al. (2009) was inferred from EUV spectroscopic measurements of the solar transition region between the photosphere and corona by Young (2005), where no elemental fractionation is observed. Note, however, that very recent measurements by Brooks et al. (2017) show evidence of fractionation even at temperatures associated with the upper transition region (~ 0.5 MK).

From a sample of X-ray observations of cool stars by *Chandra*, however, Drake & Testa (2005) brought forward some evidence in support of this higher value. They examined a sample of nearby solar-like stars, and found that a value of 0.41 for the Ne/O abundance ratio for the Sun would be in agreement with the other stars in their sample. This is a factor of 2.3–2.7 larger than the standard Ne/O abundance ratio of 0.15–0.18. Asplund et al. (2005) argued that the stellar sample of Drake & Testa (2005) was skewed toward more active stars, which show larger inverse FIP effects, a depletion of high-FIP elements rather than an enhancement of low-FIP elements (Drake et al. 2001), and that a value around 0.2 would be more reasonable for low activity stars similar to the Sun. Without a reliable solar measurement, however, it was difficult to settle this issue.

Schmelz et al. (2005) re-examined older spectroscopic data from US air force satellites and naval rocket flights in the 1960s and 70s. The measurements of full disk integrated spectra mimic what the Sun would look like if it were viewed as a star. These “Sun-as-a-star” observations allowed a direct comparison with the stellar measurements, but were found to be consistent with the standard Ne/O abundance ratio of around 0.15, apparently closing this particular avenue of exploration.

Recently, a new pathway to reconciliation has potentially emerged. Shearer et al. (2014), found that the Ne/O abundance ratio varies with the solar cycle in slow solar wind streams (< 400 km s $^{-1}$), and a similar cyclic variation was subsequently observed by Landi & Testa (2015) in coronal streamers. Although the magnitude of the variation in the slow wind is only around 40%, the variation in streamers is a factor of 2.5. Furthermore, based on the idea that the FIP effect was suppressed during the unusually extended solar minimum from 2007 to 2010, Landi & Testa (2015) argue that the higher value of 0.25 for the Ne/O abundance ratio measured at that time is closer to the true photospheric abundance. In fact, more recent studies of the abundances of oxygen and other light elements and comparison to helioseismic and solar neutrino data by Antia & Basu (2011) and Villante et al. (2014) suggest that the magnitude of the variation seen by Landi & Testa (2015) may be enough to restore agreement with the seismic data.

This conjecture remains unproven, and there are other dissenting arguments from Grevesse et al. (2013), who point out that some recent measurements of the oxygen photospheric abundance do not completely account for subtle blending

spectral lines (Caffau et al. 2011), and, in fact, that when these blends are taken into account, the O abundance is reduced. Conversely, a very recent reanalysis of quiet-Sun observations using new atomic data supports a high value of 0.24 for the Ne/O abundance ratio (Young 2018).

Recently, Brooks et al. (2017) detected a solar cyclic variation in the magnitude of the FIP effect in full disk integrated Sun-as-a-star spectra obtained by the *Solar Dynamics Observatory*. Motivated by this finding, the detections of solar cyclic variations in the Ne/O abundance ratio in the slow wind and detailed atmospheric structures, and the continuing controversy of the solar abundance problem, we decided to investigate whether the Ne/O abundance ratio depends on the solar cycle in Sun-as-a-star data. Our analysis expands on the work of Schmelz et al. (2005), with much more extensive data coverage of the solar cycle, and more recent and updated atomic data. The detection of a cyclic variation of the FIP effect in the Sun-as-a-star data suggests that this may be a promising route for solving the solar abundance problem. It also allows for a direct comparison with the stellar observations and could potentially reconcile the Sun-as-a-star Ne/O abundance ratio with that measured in nearby stars.

2. Methods

We use *SDO/EVE* (Extreme ultraviolet Variability Experiment, Woods et al. 2012) data for our analysis. EVE includes several instruments for measuring the solar EUV irradiance, including twin grating near-normal incidence spectrographs that observe in two wavelength bands from 50–370 Å and 350–1050 Å with a coarse spectral resolution of 1 Å. The short wavelength band is recorded by MEGS-A (Multiple EUV Grating Spectrographs) and the long wavelength band by MEGS-B. The observations are full disk integrated spectra. We use MEGS-A and MEGS-B level-2 v.5 spectra in this work. These data were downloaded from the Science Processing Operations Center of the Laboratory for Atmospheric and Space Physics in Colorado. The data products are fully calibrated spectra merged from the two wavelength bands. They are 10 s integrated spectral irradiance measurements that are provided as hourly data sets. We computed daily spectra by median filtering all of the spectra in the hourly data sets within each 24 hr period as in Warren (2014). We also converted the irradiance measurements from the SI units W m $^{-2}$ nm $^{-1}$ to intensities in cgs units of erg cm $^{-2}$ s $^{-1}$ sr $^{-1}$ by accounting for the solid angle, $\pi r^2/R^2$, where r is the solar radius and R is the Earth–Sun distance. The observations cover the period from 2010 April to 2014 May (1475 days in total). We show context images covering this period from the *Hinode* X-ray Telescope (XRT, Golub et al. 2007) in Figure 1.

EVE observes a large number of spectral lines covering a wide range in temperatures and we selected a set of lines that are relatively blend free (Table 1). The selection includes lines of O III–O VI, Ne V–Ne VIII, Si VII, Mg VII, Si X, and Fe IX–Fe XVI, which cover a temperature range from 0.1 MK to 2.75 MK. We extracted the intensities for all the spectral lines shown in Table 1 for each of the daily data sets. To achieve this, we integrated the intensities between pre-defined wavelength limits chosen to minimize the impact of surrounding blends. We assessed the likely impact of blends in our previous work (Brooks et al. 2017) using much higher spectral resolution observations of quiet and active regions from the EUV Imaging Spectrometer on the *Hinode* satellite (Brown

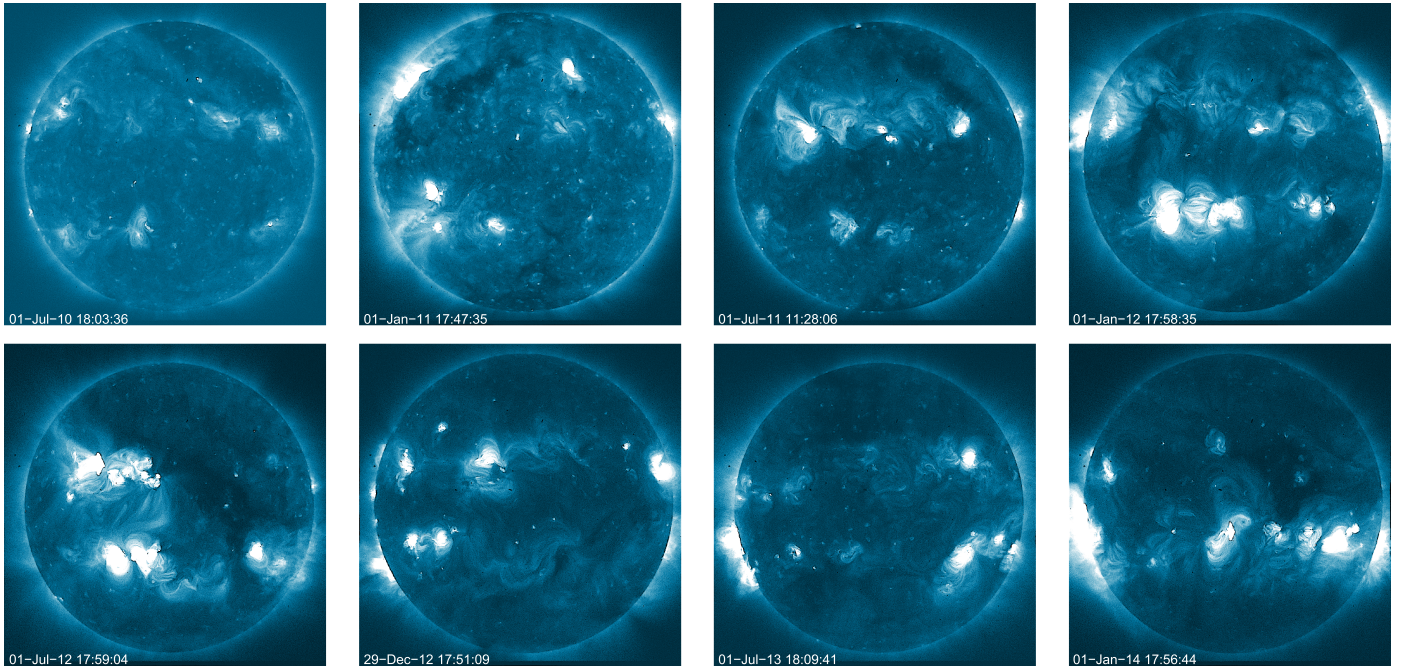


Figure 1. Sample of XRT Al-Poly images taken at 6 month intervals covering the period analyzed in this work between 2010 July and 2014 January.

Table 1
Line Selection

Line ID	$\log T_p$	Line ID	$\log T_p$
O III 599.598 Å	5.02	Si VII 275.352 Å	5.80
O IV 554.510 Å	5.22	Fe IX 171.073 Å	5.92
O V 629.730 Å	5.38	Fe X 174.532 Å	6.06
Ne V 572.311 Å	5.44	Fe X 177.239 Å	6.06
Ne V 569.820 Å	5.44	Si X 258.375 Å	6.14
O VI 1037.64 Å	5.48	Fe XI 180.401 Å	6.14
O VI 1031.93 Å	5.48	Si X 261.040 Å	6.14
Ne VII 465.221 Å	5.72	Fe XII 195.119 Å	6.20
Fe VIII 131.240 Å	5.76	Fe XIII 202.044 Å	6.24
Mg VII 278.402 Å	5.80	Fe XIV 211.316 Å	6.30
Ne VIII 780.380 Å	5.80	Fe XV 284.160 Å	6.34
Ne VIII 770.420 Å	5.80	Fe XVI 262.984 Å	6.44

Note. T_p —peak of the $G(T_p)$ function.

et al. 2008). Blending lines within 1.5 Å of the line positions mostly produce a contribution that is comparable to the assumed uncertainties. See Brooks et al. (2017) for details and exceptions.

We assume a 20% uncertainty in the intensities in our analysis (Woods et al. 2012). This is probably conservative for the lines below 750 Å, where the calibration uncertainty is likely smaller, but takes some account of uncertainties at longer wavelengths on MEGS-B that are assumed to be larger. For example, by cross-calibration between MEGS-B and the Solar EUV Experiment (SEE) on the TIMED (Thermosphere Ionosphere Mesosphere Energetics and Dynamics, Woods et al. 2005) mission, Milligan et al. (2012) were able to derive a correction factor for the 750–921 Å wavelength range during 2011 February. Applying their correction to our daily spectra taken, for example, on February 15, results in an average decrease of $\sim 20\%$ for the extracted intensities of the Ne VIII spectral lines we use in that wavelength range. This is comparable to the uncertainty we assume.

Having obtained the intensities, we followed the method of Landi & Testa (2015) to compute the Ne/O abundance ratio. The ratio of the intensities of two spectral lines, each emitted by neon and oxygen, is given by

$$\frac{I_{\text{Ne}}}{I_{\text{O}}} = \frac{\int G_{\text{Ne}}(T, n) \phi(T) dT}{\int G_{\text{O}}(T, n) \phi(T) dT}, \quad (1)$$

where T is the electron temperature, n is the electron density, ϕ is the distribution of coronal plasma with temperature, or differential emission measure, and $G(T, n)$ is the line emission contribution function. $G(T, n)$ contains all of the necessary atomic parameters and the abundance of the element, $A(Z)$, is separable from it as

$$G(T, n) = A(Z)g(T, n). \quad (2)$$

Given the electron density and emission measure distribution, the ratio $I_{\text{Ne}}/I_{\text{O}}$ can be calculated as a function of the Ne/O abundance ratio: $A(\text{Ne})/A(\text{O})$. The initial abundance ratio is assumed, and comparison with the observed ratio produces a correction to the assumed ratio. We use two sets of neon and oxygen spectral lines i.e., Ne V 572.311 Å, Ne V 569.820 Å, and O IV 554.510 Å covering the 0.17–0.28 MK temperature range, and Ne VIII 770.420 Å, Ne VIII 780.380 Å, O VI 1031.93 Å, and O VI 1037.64 Å covering the 0.3–0.63 MK temperature range. The second set of lines contains the same lines as those in Landi & Testa (2015).

To calculate the electron density and emission measure (EM) distribution, we follow a modified version of the methodology we used in previous work (Brooks & Warren 2011; Warren et al. 2011; Brooks et al. 2015). We compute the electron density using the Si X 258.375/261.04 diagnostic ratio. We then use this value to compute the $G(T, n)$ functions. Together with the observed intensities, the $G(T, n)$ functions are used to calculate the EM distribution for every daily spectrum. All the spectral lines in Table 1 were used for the EM calculations except for Ne VIII 770.420 Å and Ne VIII 780.380 Å (see Section 3.2). Technically,

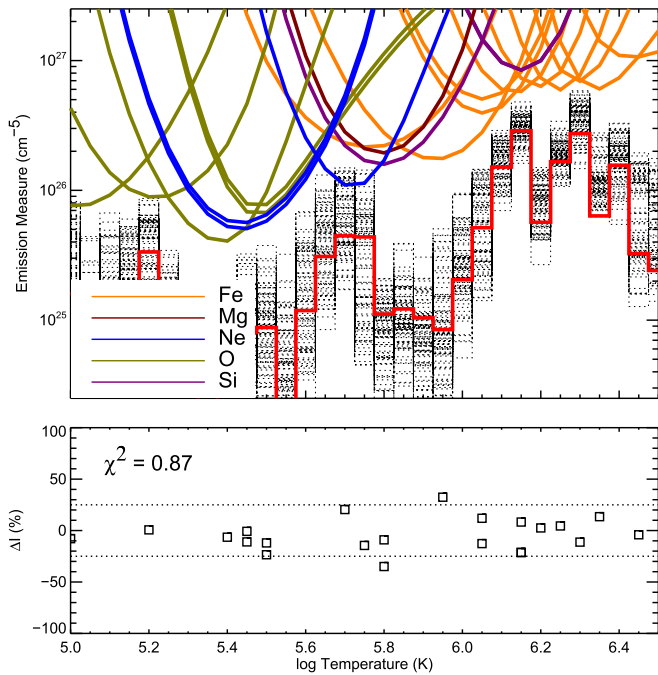


Figure 2. EM solution for the daily spectrum taken on 2012 May 4th. The best-fit EM solution is shown in red, and the Monte Carlo simulations are shown by the gray dotted lines. The colored lines are emission measure loci curves for all the spectral lines used in the calculation. The lower panel shows the differences between the observed and EM calculated intensities as a percentage of the observed intensity. They are plotted at the formation temperature of the relevant line. We show the full line-list with formation temperatures for cross-checking in Table 1. The reduced χ^2 value for the solution is shown in the legend.

we compute the EM using the Markov chain Monte Carlo (MCMC) algorithm available in the PINTofALE software package (Kashyap & Drake 1998, 2000). This technique finds the best-fit solution from 100 simulations where the observed intensities are randomly perturbed within the uncertainty. The $G(T, n)$ functions are calculated using the CHIANTI database v.8 (Dere et al. 1997; Del Zanna et al. 2015). We adopt the coronal abundances of Feldman et al. (1992) to determine the most accurate EM, though the method is insensitive to the assumed abundances since we derive a correction to them.

Once we have the EM for each data set, we compute the correction to the assumed abundances using the four independent $I_{\text{Ne}}/I_{\text{O}}$ line ratios. We take the average of the correction factors calculated for each of the four ratios.

We also compute the standard deviation of a distribution of 1000 random trials where each one finds the best-fit EM solution to 100 Monte Carlo simulations, as above, and calculates a value for the $A(\text{Ne})/A(\text{O})$ ratio. We take this standard deviation as a measure of the uncertainty in the measurements.

3. Results and Discussion

3.1. Emission Measure distributions

In Figure 2, we show an example of the EM distribution computed from the extracted intensities for the spectral lines shown in Table 1. The EM loci curves in the figure show the upper constraints on the EM. They were calculated assuming that all of the intensity is emitted from the peak formation temperature, i.e., by dividing the intensity by the contribution function. The reduced χ^2 value is close to one, which indicates

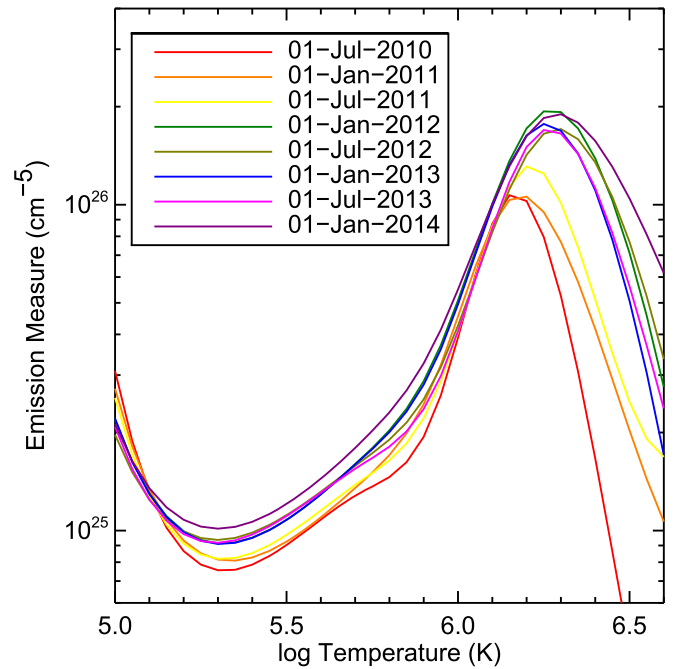


Figure 3. Sample of smoothed EM solutions taken at 6 month intervals showing the effect of the rise in solar activity between 2010 July and 2014 January. The curves are rainbow color coded from red near solar minimum to violet near solar maximum (cf. Figure 1).

that the EM model fits the observed intensities well. The differences between the EM calculated and observed intensities are less than 25% for nearly all the lines (lower panel).

We performed a similar calculation for every daily spectrum in the complete data set. There is considerable structure in the MCMC calculations, and some differences depending on which lines are included in the analysis (see below). Thus, for clarity of display and ease of comprehension of the global trends, we show a selection of EM distributions at 6 month intervals from our sample that have been post-processed by spline interpolation so that they are smoother. That is, the MCMC EM calculation for the date was used as input to a spline interpolation algorithm where several temperature/EM knot points are interactively selected, and the solution is calculated by minimizing the differences between the observed and predicted intensities (Warren 2005). The displayed distributions show the evolution of the EM from near the minimum of solar cycle 23 in 2010 July, to beyond the maximum of solar cycle 24 in 2014 January. The XRT images in Figure 1 were taken as close in time as possible to the dates shown in Figure 3. There is an enhancement in EM at all temperatures as the cycle activity increases, with the peak EM increasing from $\log \text{EM} = 26.03$ to 26.28 (a factor of nearly two). The coronal peak temperature also evolves from $\log T = 6.15$ to 6.30, corresponding to an increase from 1.4 MK near solar minimum to 2 MK near activity maximum. The EM shows much larger increases at higher temperatures, but the calculations are most uncertain in this region due to a lack of high temperature constraints above $\log T = 6.5$ in the EVE spectra.

These apparent trends are consistent with the independent analysis of *SDO* data by Morgan & Taroyan (2017), who also note a similar increase in coronal mean temperature from 1.4 MK to 1.8 MK, primarily driven by the presence and increase in a high temperature component near $\log T = 6.5$ (3 MK). Morgan & Taroyan (2017) suggest that this high

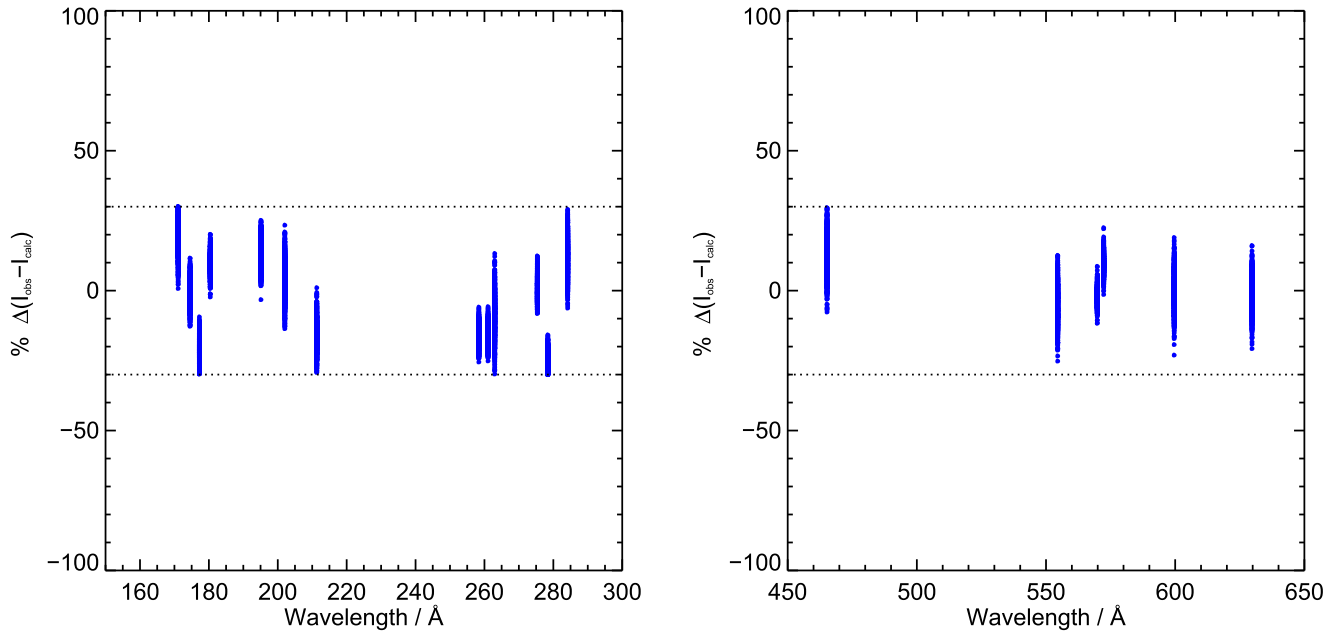


Figure 4. Difference between observed and calculated intensities expressed as a percentage of the observed intensity for all the spectral lines used in the emission measure analysis, except the those beyond 1000 Å. The data are plotted at the wavelength of the relevant line. We show the full line-list with wavelengths for cross-checking in Table 1. Results are shown for all daily spectra analyzed (1103 observations).

temperature component also leads to a solar cyclic variation in the EM distribution below $\log T = 6.2$ (1.6 MK); however, a separate analysis of EVE spectra reports that there is no variation with the solar cycle at these temperatures (Schonfeld et al. 2017). Our results are consistent with Schonfeld et al. (2017): as Figure 3 shows, the EM distribution is very similar up to at least $\log T = 6.15$ at all times. From previous work examining different spatial regions, we also do not expect much variation at these temperatures. The quiet-Sun coronal EM distribution is very similar regardless of the observing instrument when averaged over significant areas (Brooks & Warren 2006; Brooks et al. 2009). Indeed Brooks et al. (2009) suggest that it has a universal character, driven by the radiating and conducting properties of the plasma. In this picture, the explanation for the different distribution near solar maximum found by Morgan & Taroyan (2017), is that the observations at this time are not of truly quiet Sun. The EM distribution averaged over regions of quiet Sun peaks at 1.1 MK and has fallen by two orders of magnitude already by 2 MK; see, for example, Figure 6 of Brooks et al. (2009). So the composite quiet-Sun EM distribution averaged over most of the disk is contaminated by higher temperature (3 MK) activity near solar maximum, which may well be due to decaying active regions as Morgan & Taroyan (2017) suggest. The EM distribution near solar maximum should still have a universal shape, but it will be different from the usual quiet-Sun EM shape because the high temperature (different density) component is accessing a different part of the radiative loss function, which is not seen near solar minimum.

These additional data from other instruments certainly help to definitively pin down the changes at these temperatures, but the abundance diagnostics we use are sensitive to cooler plasma where the EM distribution is well constrained.

To ensure that our results are robust for all the daily spectra, we examined the differences between the observed and calculated intensities for all the spectral lines in the complete data set. Figure 4 shows these differences calculated as a

percentage of the observed intensities for all the daily spectra we used. This plot is analogous to the lower panel of Figure 2. If these differences were greater than 30% for any of the lines in a particular daily spectrum, then that date was excluded from our subsequent analysis.

3.2. Comments on the Accuracy of the Li-like Spectral Lines

There is a caveat to our threshold condition. While the atomic structure of Li-like ions is very simple (three electrons only) and lines emitted from these ions are therefore expected to be spectroscopically accurate, they are well known to sometimes show anomalously large intensities (Dupree 1972; Judge et al. 1995). Based on off-limb observations from *Hinode*/EIS, where the solar corona is close to isothermal and so atomic data discrepancies are readily apparent, Warren et al. (2016) found that the contribution functions for some O VI lines need to be adjusted upward by a factor of 3.4 to bring them into agreement with other lines. Other work has found that these discrepancies are wavelength dependent (Muglach et al. 2010), and several studies have successfully used the longer wavelength O VI lines we use here for composition studies (Feldman et al. 1998; Landi & Testa 2015).

In our analysis, we also found that the Li-like O VI 1031.93 Å, O VI 1037.64 Å, Ne VIII 770.42 Å, and Ne VIII 780.38 Å observed line intensities were several factors brighter than the intensities calculated from the EM distribution. Excluding the Ne VIII lines and adjusting the $G(T, n)$ functions for O VI 1031.93 Å and O VI 1037.64 Å upward by the factor of 3.4 determined from EIS off-limb spectra by Warren et al. (2016) improves the minimization of the EM solution, and helps to anchor the distribution around their formation temperatures. We therefore make the adjustment solely for the purpose of determining the best EM solution. We make no adjustment for the subsequent abundance ratio correction since Ne VIII is also Li-like and it is necessary to treat them consistently.

Note also that the Warren et al. (2016) adjustment factor was computed using off-limb EIS spectra taken near solar minimum in 2007, November. Our analysis suggests that this factor is also representative of the rest of the solar cycle, since the computed O VI line intensities are maintained within 25% of the observed intensities in all the daily spectra. If there was a cycle dependent variation greater than 25% in this adjustment factor, perhaps due to the presence or absence of the high temperature component in the emission measure found by Morgan & Taroyan (2017), then it would be detected in our analysis as a discrepancy between the calculated and observed intensities.

It is interesting that the same adjustment factor works well for both our EVE analysis and the independent EIS off-limb spectral analysis. For a further cross-check of consistency we have re-examined data of the quiet Sun analyzed by Warren (2005). Warren (2005) combined spectra obtained by the *SOHO* Coronal Diagnostic Spectrometer (CDS, Harrison et al. 1995) and Solar Ultraviolet Measurements of Emitted Radiation (SUMER, Wilhelm et al. 1995) instrument. Twenty spectral atlas observations of the quiet Sun were processed and added together to form the CDS part of a composite spectrum covering the 308–381 Å and 513–633 Å wavelength ranges. For SUMER, central meridian scans covering the 660–1500 Å wavelength range were used. The data are much higher spectral resolution than our EVE spectra. The CDS spectral resolution is 80 mÅ in the shorter wavelength band, and 140 mÅ in the longer wavelength band. The SUMER spectral resolution is about 45 mÅ.

Warren (2005) provided the line intensities for the composite spectrum in Tables 1 and 2. We selected 48 emission lines from their tables and computed the emission measure distribution from these intensities using the same methodology as we used for the EVE spectra. Our selection criteria was to cover the same temperature range as the EVE spectra and exclude lower temperature lines that are potentially affected by optical depth effects (see, e.g., the analysis of Brooks et al. 2000). We also excluded Li-like and Na-like lines, with the exception of the O VI lines we were testing. This was so that any discrepancy in the intensities for the O VI lines would be unaffected by the anomalous behavior of other species. Finally, we excluded lines that were not reproduced by the emission measure calculation. We therefore used lines from O III–O VI, Ne V–Ne VIII, Si IX–Si XII, Fe XI–Fe XIV, and Mg X.

We show the resulting EM distribution in Figure 5. The lower panel shows that all 48 emission line intensities are reproduced, including the O VI 1031.94 Å and O VI 1037.64 Å intensities. The figure shows the results including the factor 3.4 adjustment. We show the unadjusted EM loci curves for the O VI lines with the dashed olive curve. Without the adjustment, these lines are clearly discrepant. These results from the CDS and SUMER data are consistent with both the off-limb EIS spectra, and our analysis of all the EVE spectra. The same 3.4 adjustment factor works for all the instruments and data, and this strongly suggests that the problem lies in the atomic physics. The cross-check rules out uncertainties in the EVE calibration at these wavelengths as the source of the discrepancy.

3.3. Neon/Oxygen Abundances

Our final sample includes 1103/1475 daily spectra, and all of the line intensities in Table 1 and Figure 2 are within the

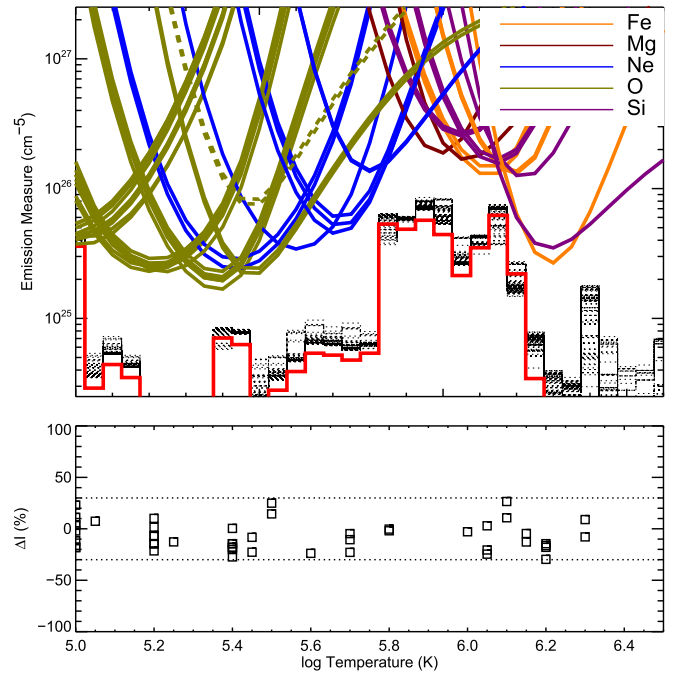


Figure 5. EM solution for the quiet-Sun spectrum from combined CDS and SUMER data. The description of Figure 2 also corresponds to this figure and the curves follow the same conventions except for the dashed curve. This is the EM loci curve for the Li-like O VI lines before adjustment (see the text).

30% limit in all of these observations. This is a much more significant data set of Sun-as-a-star observations sampling the solar cycle than any previous work. The satellite and rocket flight data used in earlier Sun-as-a-star studies had only sparse coverage of the solar cycle (Schmelz et al. 2005). While the flights in 1963–1975 did cover the minimum and maximum of solar cycle 20, and there is some suggestion that the measured $A(\text{Ne})/A(\text{O})$ ratios ranging from 0.18 to 0.25 correlate at least with the rise of the solar cycle, the value of 0.20 measured in 1969 March makes it unclear whether there is any cyclic trend.

We show our results in Figures 6 and 7. Figure 6 shows the results calculated from the Ne V/O IV ratio. The left panels show the daily and 27 day Carrington running average F10.7 cm solar radio fluxes for the period of 2008–2016 with our daily-measured $A(\text{Ne})/A(\text{O})$ ratios and 27 day Carrington running average values overlaid. The daily $A(\text{Ne})/A(\text{O})$ values fall in the range of $0.11\text{--}0.17 \pm 0.01$, decreasing from the higher value in 2010 near solar minimum when the coronal temperature was measured to be 1.4 MK, to the lower value near solar maximum in 2014 when the temperature was closer to 2 MK. The 27 day running average shows this fall less clearly, falling slightly from 0.15 in 2010 to 0.13 in 2014. That is, we find a moderate anti-correlation with the solar cycle. This is perhaps clearer to see in the 27 day running averaged data, and in the right panel of Figure 6 where we have zoomed in on the period of the EVE data. The strength of the anti-correlation can be computed from the linear Pearson correlation coefficient and is -0.54 for these data.

Figure 7 shows the results calculated from the Ne VIII/O VI ratio. The daily $A(\text{Ne})/A(\text{O})$ values fall in the range $0.08\text{--}0.16 \pm 0.01$, also decreasing from the higher value in 2010 near solar minimum to the lower value near solar maximum in 2014, and the 27 day running average values fall from 0.13 in 2010 to 0.09 in 2014. The anti-correlation with the

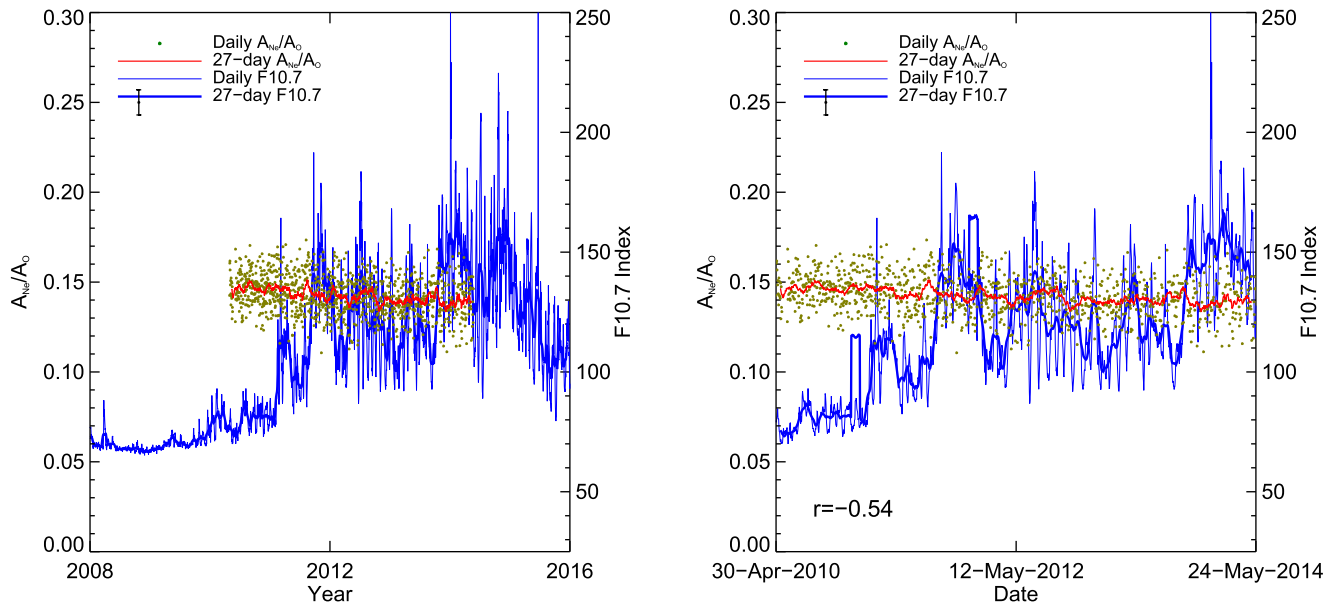


Figure 6. Left panel: F10.7 cm solar radio flux for 2008–2016 (thin blue line) with the Ne/O abundance ratios calculated from the Ne V/O IV spectral lines overlotted on the dates of the EVE daily spectra (green dots). We also show the 27 day Carrington running averaged data with the thick blue solid line (F10.7 cm) and red solid line (Ne/O abundance ratios). We show the uncertainty in the measurements with the vertical bar. Right panel: same as the left panel but zoomed in to the period of the EVE data (2010–2014). We give the linear Pearson correlation coefficient in the legend.

solar cycle is stronger at the higher temperatures associated with these spectral lines. The linear Pearson correlation coefficient is -0.68 for these data.

These results appear to indicate some fractionation between neon and oxygen over the solar cycle, despite both being high-FIP elements, as found in coronal streamers and the solar wind by Landi & Testa (2015) and Shearer et al. (2014). In fact, our results are in good agreement with the magnitude of the cyclic variations seen in the slow solar wind by Shearer et al. (2014), who found a fall from a high of 0.17 ± 0.03 at solar cycle 23 minimum to 0.12 ± 0.02 at the preceding solar cycle 23 maximum. A one-to-one comparison is not possible since the measurements cover different cycle maxima, and their measurements are 6 month mean ratios, but there is some overlap. Our measurements start from 2010, April 30, which is in the early ascending phase of the cycle and somewhat after solar minimum. Judging from their Figure 2, the value for the slow solar wind ($<350 \text{ km s}^{-1}$) is around 0.14 at this time, in agreement with ours. This also suggests that the solar minimum value for the coronal $A(\text{Ne})/A(\text{O})$ ratio may be slightly higher than our measured maximum values, i.e., our maximum values do not quite represent the truly unfractionated value. We should note also that the 27 day Carrington averaged and 6 month mean data are less likely to give us a true measure at solar minimum. This is because although days without sunspots are common near solar minimum, the Sun is less likely to be completely clear of spots for a whole month or half a year.

Since the $A(\text{Ne})/A(\text{O})$ ratio decreases with increasing activity, this would be compatible with an enhancement in the lower-FIP element oxygen compared to neon, which would be consistent with the cyclic variation of FIP-bias found in Sun-as-a-star spectra by Brooks et al. (2017). Note that Brooks et al. (2017) found a strong correlation between FIP-bias, measured from low- and high-FIP elements, and F10.7 cm flux, but the anti-correlation we find between the $A(\text{Ne})/A(\text{O})$ ratios and the 27 day running averaged F10.7 cm flux is slightly weaker during this period. This suggests that the correlation found by

Brooks et al. (2017) is driven by the behavior of the low-FIP elements with the solar cycle.

Conversely, the results are also compatible with a depletion of the higher-FIP element neon compared to oxygen. Although we consider it less likely, this could, in principle, be evidence of mass dependent fractionation due to gravitational settling of the heavier neon. Raymond et al. (1997) found evidence that plasma within large coronal loops in the equatorial streamer belt had lower abundances than the plasma at the streamer edge, and suggested this could be due to gravitational settling as a result of a longer confinement time within the closed magnetic field. Feldman et al. (1999) found other supporting evidence from measurements of line intensities as a function of height above the solar limb. In this picture, the Sun-as-a-star observations near solar minimum are dominated by emission from relatively shorter lived, and smaller, quiet-Sun loops, where gravitational settling is less likely to occur, whereas the emission near solar maximum is dominated by larger and longer-lived active region loops where gravitational settling leads to a depletion of neon relative to oxygen. It is worth pointing out that both a depletion of neon relative to oxygen due to gravitational settling, and an enhancement of the lower-FIP element oxygen, work in the same direction to decrease the $A(\text{Ne})/A(\text{O})$ ratio. So it is possible that some combination of the two effects could be at play.

3.4. Summary

In conclusion, we have used the very extensive EVE database to produce high quality daily averaged spectra covering the rise of the solar cycle from 2010 to 2014. We then used these spectra to measure the $A(\text{Ne})/A(\text{O})$ ratio in two temperature ranges and examine any solar cyclic trend when the Sun is viewed as a star. This is a much larger sampling of the solar cycle than in previous work. Using the Ne V and O IV lines, we find a relatively weak dependence on the solar cycle with a moderate anti-correlation in the Sun-as-a-star data. The measured $A(\text{Ne})/A(\text{O})$ value close to minimum is 0.17 ± 0.01

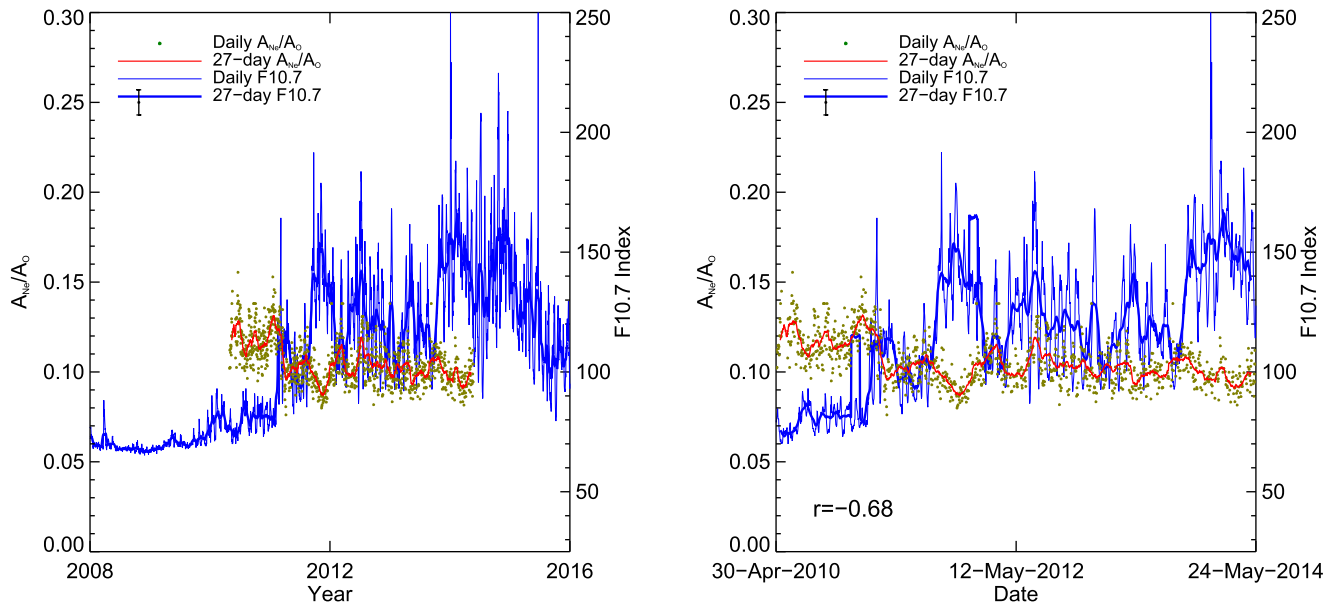


Figure 7. Same as Figure 6 but displaying the results computed from the Ne VIII/O VI ratio.

(0.15 27 day average) and the value close to maximum is 0.11 ± 0.01 (0.13 27 day average). Using the higher temperature Ne VIII and O VI lines, we find a stronger anti-correlation and a clearer cyclic variation, with a value close to minimum of 0.16 ± 0.01 (0.13 27 day average) and a value close to maximum of 0.08 ± 0.01 (0.09 27 day average).

Given the uncertainties associated with the Li-like lines, we must consider the results from the Ne V/O IV ratio to be more robust. The fact that it is sampling a lower temperature region than the Ne VIII/O VI ratio, where signatures of elemental fractionation are more difficult to detect, however, suggests that the hints of a cyclic dependence seen at those temperatures are consistent with the clearer detection in the Ne VIII/O VI measurements. In either case, the values are broadly consistent with previous measurements in the quiet Sun (Young 2005), and earlier satellite and rocket flight observations of the Sun-as-a-star (Schmelz et al. 2005), and are also consistent with measurements in the slow solar wind (Shearer et al. 2014). Our study therefore supports earlier findings that the $A(\text{Ne})/A(\text{O})$ ratio is too low to solve the “solar abundance problem” and that, given the uncertainties, it is difficult to reliably conclude that the enhancement seen at solar minimum in coronal streamers by Landi & Testa (2015), which may have helped, can be detected to a similar degree in Sun-as-a-star observations. We again, however, emphasize that our measurements do not extend fully into the deepest solar minimum of 2008–2009.

The work of D.H.B. and H.P.W. was performed under contract to the Naval Research Laboratory and was funded by the NASA *Hinode* program. D.B. and L.v.D.-G. are funded under STFC consolidated grant number ST/N000722/1. L.v.D.-G. acknowledges the Hungarian Research Grant OTKA K-109276. The authors are grateful to Konkoly Observatory, Budapest, Hungary, for hosting two workshops on Elemental Composition in Solar and Stellar Atmospheres (IFIPWS-1, 2017 February 13–15, and IFIPWS-2, 2018 February 27–March 1) and acknowledge the financial support from the Hungarian Academy of Sciences under grant NKSZ 2018_2. The workshops have fostered collaboration by exploiting synergies in solar and stellar magnetic activity studies and

exchanging experience and knowledge in both research fields. CHIANTI is a collaborative project involving George Mason University, the University of Michigan (USA) and the University of Cambridge (UK). The *SDO* data are courtesy of the NASA/*SDO*, and the AIA, EVE, and HMI science teams. *Hinode* is a Japanese mission developed and launched by ISAS/JAXA, collaborating with NAOJ as a domestic partner, NASA and STFC (UK) as international partners. Scientific operation of the *Hinode* mission is conducted by the *Hinode* science team organized at ISAS/JAXA. This team mainly consists of scientists from institutes in the partner countries. Support for the post-launch operation is provided by JAXA and NAOJ (Japan), STFC (U.K.), NASA, ESA, and NSC (Norway).

Facilities: *SDO* (EVE), *Hinode* (XRT), *SOHO* (CDS, SUMER).

ORCID iDs

BrooksDavid H.  <https://orcid.org/0000-0002-2189-9313>

BakerDeborah  <https://orcid.org/0000-0002-0665-2355>

Driel-Gesztelyi Lidia van  <https://orcid.org/0000-0002-2943-5978>

WarrenHarry P.  <https://orcid.org/0000-0001-6102-6851>

References

- Antia, H. M., & Basu, S. 2005, *ApJL*, **620**, L129
 Antia, H. M., & Basu, S. 2011, *JPhCS*, **271**, 012034
 Asplund, M., Grevesse, N., Guedel, M., & Sauval, A. J. 2005, arXiv:astro-ph/0510377
 Asplund, M., Grevesse, N., Sauval, A. J., Allende Prieto, C., & Kiselman, D. 2004, *A&A*, **417**, 751
 Asplund, M., Grevesse, N., Sauval, A. J., & Scott, P. 2009, *ARA&A*, **47**, 481
 Bahcall, J. N., Basu, S., Pinsonneault, M., & Serenelli, A. M. 2005a, *ApJ*, **618**, 1049
 Bahcall, J. N., Basu, S., & Serenelli, A. M. 2005b, *ApJ*, **631**, 1281
 Bahcall, J. N., Pinsonneault, M. H., Basu, S., & Christensen-Dalsgaard, J. 1997, *PhRvL*, **78**, 171
 Brooks, D. H., Baker, D., van Driel-Gesztelyi, L., & Warren, H. P. 2017, *NatCo*, **8**, 183
 Brooks, D. H., Ugarte-Urra, I., & Warren, H. P. 2015, *NatCo*, **6**, 5947
 Brooks, D. H., & Warren, H. P. 2006, *ApJS*, **164**, 202

- Brooks, D. H., & Warren, H. P. 2011, [ApJL](#), **727**, L13
- Brooks, D. H., Warren, H. P., Williams, D. R., & Watanabe, T. 2009, [ApJ](#), **705**, 1522
- Brooks, D. H., Fischbacher, G. A., Fludra, A., et al. 2000, [A&A](#), **357**, 697
- Brown, C. M., Feldman, U., Seely, J. F., Korendyke, C. M., & Hara, H. 2008, [ApJS](#), **176**, 511
- Caffau, E., Ludwig, H.-G., Steffen, M., Freytag, B., & Bonifacio, P. 2011, [SoPh](#), **268**, 255
- Del Zanna, G., Dere, K. P., Young, P. R., Landi, E., & Mason, H. E. 2015, [A&A](#), **582**, A56
- Dere, K. P., Landi, E., Mason, H. E., Monsignori Fossi, B. C., & Young, P. R. 1997, [A&AS](#), **125**, 149
- Drake, J. J., Brickhouse, N. S., Kashyap, V., et al. 2001, [ApJL](#), **548**, L81
- Drake, J. J., & Testa, P. 2005, [Natur](#), **436**, 525
- Dupree, A. K. 1972, [ApJ](#), **178**, 527
- Fabbian, D., Khomenko, E., Moreno-Insertis, F., & Nordlund, Å. 2010, [ApJ](#), **724**, 1536
- Fabbian, D., Moreno-Insertis, F., Khomenko, E., & Nordlund, Å. 2012, [A&A](#), **548**, A35
- Feldman, U., Doschek, G. A., Schühle, U., & Wilhelm, K. 1999, [ApJ](#), **518**, 500
- Feldman, U., Mandelbaum, P., Seely, J. F., Doschek, G. A., & Gursky, H. 1992, [ApJS](#), **81**, 387
- Feldman, U., Schühle, U., Widing, K. G., & Laming, J. M. 1998, [ApJ](#), **505**, 999
- Golub, L., DeLuca, E., Austin, G., et al. 2007, [SoPh](#), **243**, 63
- Grevesse, N., Asplund, M., Sauval, J., & Scott, P. 2013, [EPJWC](#), **43**, 01004
- Grevesse, N., Noels, A., & Sauval, A. J. 1996, in ASP Conf. Ser. 99, Cosmic Abundances, ed. S. S. Holt & G. Sonneborn (San Francisco, CA: ASP), 117
- Harrison, R. A., Sawyer, E. C., Carter, M. K., et al. 1995, [SoPh](#), **162**, 233
- Judge, P. G., Woods, T. N., Brekke, P., & Rottman, G. J. 1995, [ApJL](#), **455**, L85
- Kashyap, V., & Drake, J. J. 1998, [ApJ](#), **503**, 450
- Kashyap, V., & Drake, J. J. 2000, [BASI](#), **28**, 475
- Landi, E., & Testa, P. 2015, [ApJ](#), **800**, 110
- Meyer, J.-P. 1985, [ApJS](#), **57**, 173
- Milligan, R. O., Chamberlin, P. C., Hudson, H. S., et al. 2012, [ApJL](#), **748**, L14
- Morgan, H., & Taroyan, Y. 2017, [SciA](#), **3**, e1602056
- Muglach, K., Landi, E., & Doschek, G. A. 2010, [ApJ](#), **708**, 550
- Nordlund, Å., Stein, R. F., & Asplund, M. 2009, [LRSP](#), **6**, 2
- Pottasch, S. R. 1963, [ApJ](#), **137**, 945
- Raymond, J. C., Kohl, J. L., Noci, G., et al. 1997, [SoPh](#), **175**, 645
- Schmelz, J. T., Nasraoui, K., Roames, J. K., Lippner, L. A., & Garst, J. W. 2005, [ApJL](#), **634**, L197
- Schmelz, J. T., Saba, J. L. R., Ghosh, D., & Strong, K. T. 1996, [ApJ](#), **473**, 519
- Schonfeld, S. J., White, S. M., Hock-Mysliwiec, R. A., & McAteer, R. T. J. 2017, [ApJ](#), **844**, 163
- Shearer, P., von Steiger, R., Raines, J. M., et al. 2014, [ApJ](#), **789**, 60
- Villante, F. L., Serenelli, A. M., Delahaye, F., & Pinsonneault, M. H. 2014, [ApJ](#), **787**, 13
- Warren, H. P. 2005, [ApJS](#), **157**, 147
- Warren, H. P. 2014, [ApJL](#), **786**, L2
- Warren, H. P., Brooks, D. H., Doschek, G. A., & Feldman, U. 2016, [ApJ](#), **824**, 56
- Warren, H. P., Brooks, D. H., & Winebarger, A. R. 2011, [ApJ](#), **734**, 90
- Wilhelm, K., Curdt, W., Marsch, E., et al. 1995, [SoPh](#), **162**, 189
- Woods, T. N., Eparvier, F. G., Bailey, S. M., et al. 2005, [JGRA](#), **110**, A01312
- Woods, T. N., Eparvier, F. G., Hock, R., et al. 2012, [SoPh](#), **275**, 115
- Young, P. R. 2005, [A&A](#), **444**, L45
- Young, P. R. 2018, [ApJ](#), **855**, 15